HHS Public Access

Author manuscript

Nat Neurosci. Author manuscript; available in PMC 2011 December 01.

Published in final edited form as:

Nat Neurosci. 2011 June ; 14(6): 750–756. doi:10.1038/nn.2801.

Neuronal activity regulates the regional vulnerability to amyloid-β deposition

Adam W. Bero[1,2,6,7], **Ping Yan**[1,6,7], **Jee Hoon Roh**[1,2,6,7], **John R. Cirrito**[1,6,7], **Floy R. Stewart**[1,2,6,7], **Marcus E. Raichle**[1,3,4,5], **Jin-Moo Lee**[1,6,7], and **David M. Holtzman**[1,2,6,7]

[1] Department of Neurology, Washington University School of Medicine, St. Louis, MO, 63110, USA

[2] Department of Developmental Biology, Washington University School of Medicine, St. Louis, MO, 63110, USA

[3] Department of Radiology, Washington University School of Medicine, St. Louis, MO, 63110, USA

[4] Department of Anatomy and Neurobiology, Washington University School of Medicine, St. Louis, MO, 63110, USA

[5] Department of Biomedical Engineering, Washington University School of Medicine, St. Louis, MO, 63110, USA

[6] Hope Center for Neurological Disorders, Washington University School of Medicine, St. Louis, MO, 63110, USA

[7] Charles F. and Joanne Knight Alzheimer's Disease Research Center, Washington University School of Medicine, St. Louis, MO, 63110, USA

Abstract

Amyloid-β (Aβ) plaque deposition in specific brain regions is a major pathological hallmark of Alzheimer'fs disease (AD). However, the mechanism underlying the regional vulnerability to Aβ deposition in AD is unknown. Herein, we provide evidence that endogenous neuronal activity regulates the regional concentration of interstitial fluid (ISF) Aβ which drives local Aβ aggregation. Using in vivo microdialysis, we show that ISF Aβ levels in multiple brain regions of APP transgenic mice prior to plaque deposition were commensurate with the degree of subsequent plaque deposition and to the concentration of lactate, a marker of neuronal activity. Furthermore,

To whom correspondence should be addressed: David M. Holtzman, M.D., Andrew B. and Gretchen P. Jones Professor and Chair, Department of Neurology, Washington University School of Medicine, 660 S. Euclid Ave. Campus Box 8111, Saint Louis, MO 63110, Administrator phone: (314) 747-0644, Office phone: (314) 362-9872, Fax: (314) 362-2244, holtzman@neuro.wustl.edu.

AUTHOR CONTRIBUTIONS

A.W.B., M.E.R, J-M.L. and D.M.H. conceived and designed the study. A.W.B. performed Aβ immunohistochemistry, plaque quantification, steady-state microdialysis, $A\beta_{x\text{-}40}$ and $A\beta_{x\text{-}42}$ ELISA assays, lactate assays, western blots, ISF Aβ $t_{1/2}$ microdialysis, vibrissae deprivation microdialysis and vibrissae stimulation microdialysis experiments. P.Y. performed long-term vibrissae deprivation, multiphoton microscopy and double immunofluorescence experiments. J.H.R. performed sleep/wake experiments, $A\beta_{1\text{-}X}$ ELISA assays and lactate assays. F.R.S. harvested brain tissue and performed X-34 staining. J.R.C. performed sequential PTX-TTX infusion microdialysis experiments. All of the authors discussed the results. A.W.B. wrote the manuscript with critical evaluation from all authors.

unilateral vibrissae stimulation increased ISF Aβ, and unilateral vibrissae deprivation decreased ISF Aβ and lactate levels in contralateral barrel cortex. Long term unilateral vibrissae deprivation decreased amyloid plaque formation and growth. Our results suggest a mechanism to account for the vulnerability of specific brain regions to Aβ deposition in AD.

Alzheimer's disease (AD) is the most common type of dementia and is characterized by insidious degeneration of brain systems that subserve memory and cognition. Accumulation and aggregation of the amyloid-β (Aβ) peptide in the extracellular space of the brain is a major pathological hallmark of AD. Aβ is produced in neurons by sequential proteolytic cleavage of the amyloid precursor protein (APP) by β- and γ-secretase[1]. Under normal conditions, Aβ is secreted into the interstitial fluid (ISF) of the brain where it is present in a soluble form throughout life[2]. In AD pathogenesis, Aβ aggregates into higher-order species such as soluble oligomers and insoluble amyloid plaques in a concentration-dependent manner. As amyloid plaques are extracellular structures, the concentration of Aβ in the ISF is likely a key determinant of whether and when Aβ will aggregate[3]. Consistent with this hypothesis, we have recently shown that ISF Aβ concentration is closely associated with amyloid plaque growth and formation in vivo[4].

In AD brain, amyloid plaque deposition is most prominent in the "default-mode network" -a network of brain regions that exhibits elevated metabolic activity and aerobic glycolysis in the resting state[5–10]. Indeed, default network dysfunction is present in AD patients[11] as well as cognitively normal adults who harbor significant amyloid burden[12, 13]. However, the mechanism underlying the vulnerability of specific brain regions to amyloid deposition in AD is not known. Given the near 1:1 stoichiometry between neuronal energy consumption and neurotransmitter cycling in vivo[14], this correspondence raises the possibility of a relationship between patterns of neuronal activity throughout life and the topology of amyloid deposition in AD. Evidence from our laboratory and others suggests that synaptic activity regulates Aβ production and secretion into the ISF in vitro[15, 16] and in vivo[17, 18]. For example, electrical stimulation of the perforant pathway increases ISF Aβ levels in hippocampus, while blockade of synaptic vesicle exocytosis decreases ISF Aβ levels. However, the relationship between endogenous regional differences in neuronal activity and amyloid deposition remains unknown. Herein, we provide data that suggests that regional differences in endogenous neuronal activity dynamically regulate Aβ levels and have implications in the development of Aβ-related pathology.

RESULTS

Regional plaque deposition in aged Tg2576 mouse brain

Aggregation of Aβ into amyloid plaques in the extracellular space of the brain is a pathological signature of AD. In AD, amyloid deposition is most prominent in brain areas that comprise the "default network": a network of anatomically defined brain regions preferentially active during undirected mentation. Core regions of the default network in human cortex include medial and lateral parietal, posterior cingulate, retrosplenial, medial prefrontal areas as well as the hippocampal formation. Though region-specific Aβ deposition is a fundamental feature of AD pathology, the mechanisms that underlie this effect are not

known. To begin to elucidate the mechanisms that regulate region-specific amyloid deposition, we first characterized the distribution of Aβ deposition in APP transgenic (Tg2576[19]) mice, which express a mutated form of amyloid precursor protein (APP). Brain sections from 17.5 ± 0.5 month-old Tg2576 mice were immunostained with biotinylated-3D6 antibody (anti $A\beta_{1-5}$) to determine the percent area occupied by Aβ plaques in multiple brain regions of interest. We found a stepwise increase in Aβ plaque burden across barrel (3.96 ± 0.69), cingulate (9.00 ± 1.59) and piriform (16.54 ± 4.07) cortices (Fig. 1a–c). Aβ plaque burden in hippocampus (5.51 ± 1.45) was similar to barrel cortex while striatum (0.62 ± 0.11) exhibited the lowest level of plaque deposition of all regions examined (Fig. 1a–c). Tg2576 mice thus exhibit region-specific Aβ deposition that is quite similar to the pattern observed in human AD.

To determine whether fibrillar amyloid plaques exhibited a distribution similar to Aβ immunopositive plaques, brain sections from aged Tg2576 mice were stained with the amyloid-specific dye, X-34. In accord with the pattern of Aβ immunopositive plaque deposition, we found that the percent area occupied by X-34-positive amyloid plaque deposition exhibited a stepwise increase in barrel (0.27 ± 0.03), cingulate (1.22 ± 0.34) and piriform (2.90 ± 0.40) cortices (Fig. 1d–f,i). Amyloid deposition in hippocampus (0.43 ± 0.09) was similar to barrel cortex (Fig. 1g,i). Amyloid was not detected in striatum (Fig. 1h,i). These results suggest that regional differences in Aβ and amyloid plaque deposition are present in aged Tg2576 mouse brain and that Tg2576 mice represent a useful model in which to examine mechanisms underlying regional vulnerability to Aβ and amyloid plaque deposition.

ISF Aβ levels predict region-specific plaque deposition

Under normal physiological conditions, Aβ is produced in neurons by sequential proteolytic cleavage of APP and is secreted into the ISF in a soluble form. During AD pathogenesis, Aβ aggregates into higher-order species in a concentration-dependent manner. As we have previously demonstrated that the concentration of Aβ in the ISF is closely associated with amyloid plaque growth and formation in vivo, we hypothesized that the steady-state concentration of ISF Aβ in each brain region early in life prior to plaque deposition would be predictive of the degree of subsequent plaque deposition in aged mice. To test this hypothesis, we performed in vivo microdialysis to measure steady-state ISF Aβ levels in multiple brain regions of young (3.5 ± 0.5 month-old) Tg2576 mice prior to the onset of plaque deposition. We found that steady-state ISF $A\beta_{x\text{-}40}$ levels were greatest in piriform cortex (2296.55 ± 308.35 pg ml^{-1}), intermediate in barrel cortex (824.16 ± 112.81) and hippocampus (1150.10 ± 130.71) and lowest in striatum (184.74 ± 25.71; Fig. 2a). ISF $A\beta_{x\text{-}40}$ levels in young mice prior to plaque deposition are therefore predictive of the level of both Aβ (Fig. 2b) and fibrillar amyloid (Fig. 2c) plaque deposition in aged mice in a region-specific manner. We next sought to determine whether the concentration of the more amyloidogenic form of Aβ, $A\beta_{x\text{-}42}$, in each brain region of young mice was predictive of the level of plaque deposition in aged mice. Consistent with our data regarding regional ISF $A\beta_{x\text{-}40}$ levels, we found that ISF $A\beta_{x\text{-}42}$ concentration was greatest in piriform cortex (104.94 ± 30.21 pg ml^{-1}), intermediate in barrel cortex (48.24 ± 6.79) and hippocampus (44.31 ± 8.25) and lowest in striatum (9.47 ± 1.46; Fig. 2d). Therefore, regional ISF $A\beta_{x\text{-}42}$

concentration in young mice is also predictive of the degree of regional Aβ (Fig. 2e) and amyloid (Fig. 2f) plaque deposition in aged mice.

Next, we assessed whether regional differences in ISF Aβ levels were present in young wild-type (B6SJL) mice. In accord with our findings in APP transgenic mice, murine ISF $A\beta_{x\text{-}40}$ levels were significantly greater in hippocampus (148.51 ± 17.93 pg ml^{-1}) compared to striatum (47.4 ± 11.46; $P = 0.0032$; Supplementary Fig. 1a). This result suggests that regional differences in ISF Aβ concentration are intrinsic to normal brain physiology. Together, these data suggest that steady-state ISF Aβ levels in young mice are predictive of the degree of Aβ and amyloid plaque deposition in a region-specific manner.

ISF lactate levels predict region-specific ISF Aβ levels

In AD, amyloid plaques preferentially deposit in brain regions that constitute the default network. As the default network exhibits elevated cerebral metabolism during resting state conditions, one possibility is that elevated metabolic activity in specific brain regions throughout life regulates the ultimate distribution of amyloid deposition. Previous data suggests that synaptic activity regulates soluble extracellular Aβ levels in vitro and in vivo. As ISF Aβ concentration is closely associated with amyloid plaque growth and formation, we hypothesized that regional differences in baseline neuronal activity would be proportional to regional steady-state ISF Aβ concentration in Tg2576 mice prior to the onset of plaque deposition. Previous data suggests that neuronal activity directly regulates extracellular lactate concentration in vitro[20] and in vivo[21]. To further establish ISF lactate as a marker of neuronal activity, we performed pharmacological manipulation of neuronal activity during in vivo microdialysis with concurrent intraparenchymal EEG recording in young Tg2576 mice. To determine whether increased neuronal activity increased ISF lactate and Aβ levels, we administered picrotoxin (12.5 μM; PTX), a $GABA_A$ receptor antagonist, via reverse microdialysis. Infusion of PTX into hippocampus increased hippocampal EEG amplitude (Fig. 3a) and ISF lactate levels compared to basal conditions (PTX, 129.6 ± 6.4; basal, 100.0 ± 8.76; $P = 0.0342$; Fig. 3b; Supplementary Figure 2a). In accord with previous data[18], PTX also significantly increased hippocampal ISF $A\beta_{x\text{-}40}$ concentration relative to basal conditions (PTX, 125.8 ± 5.16; basal, 100.0 ± 5.21; $P = 0.0126$; Fig. 3c; Supplementary Figure 2b). To determine whether depression of local neuronal activity reduces ISF lactate and Aβ levels, we administered the voltage-gated sodium channel blocker, tetrodotoxin (5 μM; TTX) via reverse microdialysis. Compared to basal conditions, TTX reduced EEG amplitude (Fig. 3a) and ISF lactate levels in hippocampus (TTX, 69.62 ± 2.69; basal, 100.0 ± 8.75; $P = 0.0160$; Fig. 3b; Supplementary Figure 2a). Consistent with previous data[17], TTX infusion also reduced ISF $A\beta_{x\text{-}40}$ concentration (TTX, 67.11 ± 2.94; basal, 100.0 ± 5.21; $P = 0.0015$; Fig. 3c; Supplementary Figure 2b). Across basal, PTX treatment and TTX treatment conditions, ISF lactate levels were significantly correlated with ISF Aβ levels (Pearson $r = 0.7645$; $P < 0.0001$; Fig. 3d). Together, these data suggest that increasing neuronal activity increases, and decreasing neuronal activity decreases, ISF lactate concentration and suggest that ISF lactate is a marker of neuronal activity in vivo.

To test the hypothesis that regional differences in ISF lactate are proportional to regional steady-state ISF Aβ concentration prior to the onset of plaque deposition, we next performed

in vivo microdialysis to measure steady-state ISF lactate level in multiple brain regions of young Tg2576 mice. We found that ISF lactate level was greatest in piriform cortex (142.47 ± 10.19), intermediate in barrel cortex (124.94 ± 11.58) and hippocampus (119.3 ± 10.53) and lowest in striatum (100.0 ± 11.93). ISF lactate levels were thus commensurate with steady-state ISF $A\beta_{x-40}$ (Fig. 4a) and $A\beta_{x-42}$ (Fig. 4b) levels in young Tg2576 mice. Moreover, steady-state ISF lactate levels were proportional to the level of subsequent Aβ (Fig. 4c) and amyloid (Fig. 4d) plaque deposition in a region-specific manner. To test whether the relationship between basal ISF lactate and ISF Aβ levels was also present in wild-type mice, we measured ISF lactate levels in hippocampus and striatum of young B6SJL mice. In accord with our data in Tg2576 mice, ISF lactate level was closely associated with murine ISF $A\beta_{x-40}$ concentration in young B6SJL mice (Supplementary Fig. 1b). These results suggest that regional differences in ISF lactate in young mice prior to plaque deposition are closely associated with steady-state ISF Aβ concentration and subsequent plaque deposition in Tg2576 mice.

ISF Aβ $t_{1/2}$ does not differ across brain regions

As steady-state ISF Aβ concentration is the result of a balance between the rates of Aβ production and clearance, we next sought to determine whether regional differences in ISF Aβ clearance rate might be associated with steady-state ISF Aβ levels in young Tg2576 mice and might therefore contribute to region-specific Aβ deposition. To assess this possibility, we performed in vivo microdialysis in multiple brain regions of young Tg2576 mice. During the microdialysis sampling period, mice were treated intraperitoneally with Compound E (10 mg kg^{-1}), a potent γ-secretase inhibitor, to rapidly halt Aβ synthesis and permit determination of ISF Aβ elimination half-life ($t_{1/2}$) as previously described[2]. ISF $A\beta_{x-40}$ $t_{1/2}$ did not differ significantly across barrel cortex (0.99 ± 0.11 hr), hippocampus (0.97 ± 0.03) and striatum (1.21 ± 0.08; $P = 0.1175$) in the brain of young Tg2576 mice (Supplementary Fig. 3a,b), suggesting that regional variation in ISF Aβ clearance rate is not sufficient to account for the pattern of plaque deposition in aged Tg2576 mice.

APP processing does not predict regional ISF Aβ levels

Amyloidogenic processing of full-length APP by β- and γ-secretase is necessary for Aβ generation. β-secretase cleavage of APP holoprotein produces C-terminal fragment (CTF)-β while non-amyloidogenic processing of APP by α-secretase produces CTF-α and precludes Aβ generation. Differential expression or processing of APP holoprotein across brain regions could thus contribute to regional differences in steady-state ISF Aβ levels and plaque deposition. To test this possibility, we performed western blot analyses to assess levels of APP holoprotein, CTF-β and CTF-α across cortical regions that harbor differential ISF Aβ levels and develop differential plaque burden. Despite dramatic differences in steady-state ISF Aβ levels and plaque deposition, expression levels of full-length APP, CTF-β and CTF-α were similar in piriform, cingulate and barrel cortices ($P = 0.9437$, 0.9821 and 0.6348 for APP, CTF-β and CTF-α, respectively; Supplementary Fig. 4a–c). To determine the role of APP expression and processing in region-specific regulation of Aβ concentration in subcortical structures, we next measured the levels of APP holoprotein, CTF-β and CTF-α in whole cortex, hippocampus and striatum. Relative to hippocampus and striatum, APP holoprotein expression was significantly greater in cortex ($P = 0.0017$; Supplementary Fig.

4d,f). CTF-β expression was significantly lower in striatum relative to hippocampus (P = 0.0245; Supplementary Fig. 4e,f), while CTF-α expression did not differ across cortex, hippocampus and striatum (P = 0.9761; Supplementary Fig. 4e,f). Together, these results suggest that regional APP expression and processing profiles are not associated with local steady-state ISF Aβ levels or plaque deposition and are thus not sufficient to account for the pattern of amyloid deposition observed in Tg2576 mice.

Vibrissal activity regulates ISF Aβ levels

The present data suggest that regional differences in basal ISF lactate levels are closely associated with steady-state ISF Aβ levels and are predictive of subsequent plaque deposition. We next sought to determine whether a causal relationship between physiological neuronal activity and both steady-state ISF Aβ and lactate concentrations exists in vivo. In rodents, each vibrissa is somatotopically mapped onto a defined cluster of neurons termed a “barrel” in primary somatosensory cortex[22]. There, neurons in each barrel respond to stimulation of the vibrissa to which they are synaptically connected. Vibrissa stimulation increases[23], while vibrissa removal decreases[24], neuronal activity in barrel cortex. Therefore, the vibrissae-barrel system represents a noninvasive physiological circuit in which to examine the relationship between physiological neuronal activity and ISF Aβ levels in vivo.

To determine whether a manipulation which causes a physiological reduction in neuronal activity could reduce ISF Aβ levels, we performed vibrissae deprivation during in vivo microdialysis in barrel cortex of young Tg2576 mice. After establishing stable basal ISF Aβ levels, all vibrissae contralateral to the microdialysis probe were trimmed to within 1 mm of the facial pad. Acute vibrissae trimming reduced ISF Aβ levels in barrel cortex by 22% compared to baseline (P = 0.0107; Fig. 5a,c). Similarly, vibrissae trimming reduced ISF lactate levels in barrel cortex by 19% relative to basal conditions (P = 0.0127; Fig. 5b,c).

To determine whether a manipulation which causes a physiological increase in neuronal activity is sufficient to increase ISF Aβ levels, we next performed unilateral mechanical vibrissae stimulation during in vivo microdialysis in barrel cortex of a separate cohort of young Tg2576 mice anesthetized with ketamine-xylazine (130.4 and 20.1 mg kg^{-1}, respectively). Ketamine-xylazine was chosen as the anesthetic agent since both basal and vibrissae stimulation-induced neurophysiological responses under ketamine-xylazine anesthesia resemble the responses elicted during wake and quiet sleep more closely than other forms of anesthesia[25]. We found that unilateral mechanical vibrissae stimulation (5–7 Hz, 4 s burst, 4 s inter-burst interval) for 30 minutes increased ISF $Aβ_{x-40}$ levels in barrel cortex by 31% relative to control conditions (P = 0.0446; Fig. 5d).

ISF lactate levels exhibit diurnal fluctuation

The sleep/wake cycle is associated with diurnal fluctuation of ISF Aβ; ISF Aβ concentration is greater during wakefulness and lesser during sleep[26]. Previous data from humans and animal models suggest that periods of wakefulness are associated with increased synaptic strength and periods of sleep are associated with decreased synaptic strength[27–29]. Therefore, we reasoned that diurnal fluctuation of ISF Aβ levels might be linked with lactate

levels throughout the sleep/wake cycle. To assess this possibility, we performed in vivo microdialysis in hippocampus of young Tg2576 housed in 12 hour light/12 hour dark conditions. Consistent with our previous findings, ISF $A\beta_{1\text{-}X}$ levels were 21% greater during the dark period relative to the light period ($P = 0.0314$; Fig. 6a,c). Moreover, ISF lactate levels were 23% greater during the dark period compared to the light period ($P = 0.0066$; Fig. 6b,c). ISF $A\beta_{1\text{-}X}$ levels were thus correlated with ISF lactate levels throughout the sleep/wake cycle (Pearson r = 0.6351; $P < 0.0001$; Fig. 6d). As animals spent significantly more time awake during the dark period compared to the light period (dark, 51.32 ± 1.26 minutes awake per hour; light, 25.02 ± 2.15; $P < 0.0001$), these findings suggest that wakefulness, ISF lactate, and ISF Aβ are co-regulated and are consistent with the hypothesis that diurnal fluctuation in neuronal activity contributes to the diurnal fluctuation of ISF Aβ levels in vivo.

Vibrissae deprivation reduces plaque formation and growth

We have previously demonstrated that the concentration of ISF Aβ is closely related to amyloid plaque growth and formation in vivo. As our present data suggest that acute manipulations that alter neuronal activity modulate ISF Aβ concentration, we hypothesized that manipulations that cause longer-term changes in neuronal activity might modulate amyloid plaque growth and formation in vivo. To test this hypothesis, we utilized 7 month-old APPswe/PSEN1ΔE9 (APP/PS1[30]) bitransgenic mice since this strain develops aggressive fibrillar amyloid deposition beginning at 4–5 months of age. Using in vivo multiphoton microscopy, amyloid plaques in barrel cortex of each hemisphere were visualized with methoxy-X04 under thinned-skull cranial windows to obtain basal measures of individual amyloid plaque size. All vibrissae on the right side of the facial pad were subsequently trimmed to within 1 mm of the face every other day for 28 days. At the conclusion of the 28-day vibrissae deprivation period, amyloid plaques in barrel cortex of each hemisphere were re-imaged to assess the effect of vibrissae deprivation on individual amyloid plaque growth. We found that plaque growth was decreased by 78% in the vibrissae-deprived relative to the control hemisphere ($P = 0.0014$; Fig. 7a–e). Moreover, new amyloid plaque formation was decreased by 65% in the deprived relative to the control hemisphere ($P = 0.0367$; Fig. 7a–d,f).

To determine whether suppression of amyloid plaque growth and formation following long-term vibrissae deprivation might be attributable to increased glial activation in barrel cortex, brains were sectioned and stained for GFAP and Iba-1 to visualize astrocytic and microglial activation, respectively. Confocal microscopy revealed no qualitative difference in astrocytic (Supplementary Fig. 5a–c) or microglial (Supplementary Fig. 5d–f) activation in the deprived hemisphere compared to the control hemisphere. This result suggests that altered glial activation is not likely to contribute to the observed suppression of amyloid plaque growth and formation following long-term vibrissae deprivation. Taken together, while long-term vibrissae deprivation results in several changes in the brain, the present data are consistent with the hypothesis that physiological neuronal activity regulates amyloid plaque growth dynamics in vivo.

DISCUSSION

Aggregation of Aβ into higher-order structures such as extracellular amyloid plaques is a necessary event in AD pathogenesis. A fundamental feature of AD is the preferential deposition of amyloid plaques in distinct brain regions. However, the mechanism by which specific brain regions are rendered vulnerable to amyloid deposition in AD has heretofore remained unknown. As Aβ aggregation is closely related to ISF Aβ concentration in vivo, elucidating the mechanisms that regulate ISF Aβ levels has important implications for understanding the etiology of region-specific Aβ deposition in AD. In the present work, we utilize in vivo microdialysis to show that ISF Aβ levels measured in several brain regions of young Tg2576 mice months prior to plaque deposition are directly proportional to the degree of subsequent plaque deposition. Moreover, ISF Aβ levels in young mice are closely associated with the level of baseline ISF lactate, a marker of neuronal activity, in a region-specific manner. Furthermore, we show that physiological changes in neuronal activity are sufficient to dynamically modulate ISF Aβ levels and amyloid plaque growth in vivo. Collectively, our results suggest that regional differences in basal neuronal activity level govern region-specific amyloid deposition through long-term regulation of steady-state ISF Aβ concentration.

Since sequential proteolysis of APP by β- and γ-secretase is necessary for Aβ generation, several previous reports have examined the regional distribution of this triad as potential mediators of region-specific Aβ deposition. However, the cerebral distribution of APP, BACE1 and PS1 transcripts is not associated with the topology of Aβ deposition in human AD[31–34] or APP transgenic mice[35–37]. Moreover, the regional distribution of γ-secretase activity in APP transgenic mouse brain does not correlate with the pattern of Aβ deposition[38]. Consistent with these previous reports, the present results suggest that though differences in APP expression and processing are present across a subset of brain areas in Tg2576 mice, the pattern of APP expression and processing is not sufficient to account for the pattern of Aβ deposition. Together, these studies suggest that additional factors are necessary to drive region-specific Aβ deposition. In addition to region-specific differences in neuronal activity potentially contributing to region-specific differences in Aβ deposition, other possible contributors to the presence of Aβ in specific neural networks include the spreading of Aβ aggregates within and into the brain. For instance, exogenously applied Aβ aggregates can seed cerebral β-amyloidosis via intracerebral[3, 39] or peripheral[40] application. Further, reports suggest that selective overexpression of APP in the cell bodies of neurons in the entorhinal cortex of transgenic mice can produce elevated soluble Aβ levels and amyloid plaque deposition in the synaptic terminal zone of the dentate gyrus[41, 42]. Thus, transsynaptic propagation mechanisms as well as spread of Aβ pathology through interconnected neural networks might also contribute to the pattern of amyloid deposition observed in AD.

In healthy human brain, a specific subset of brain regions – the default network – is preferentially engaged during resting state conditions. Intriguingly, amyloid deposition in AD brain is most prominent in regions that comprise the default network. These findings raise the possibility that patterns of normal cerebral metabolism may influence the distribution of amyloid deposition in AD. In accord with this hypothesis, recent data

suggests that the spatial distribution of resting state aerobic glycolysis (i.e. glucose utilization in excess of that used for oxidative phosphorylation despite sufficient oxygen to oxidize glucose to carbon dioxide and water) in cognitively normal adults overlaps closely with the topology of amyloid deposition in AD. Our present data demonstrating that pharmacological manipulation of neuronal activity directly regulates ISF lactate levels are consistent with previous animal and human studies and suggest that neuronal activity stimulates aerobic glycolysis in vivo. Given that neuronal activity also increases Aβ production and secretion into the ISF, regional differences in neuronal activity may underlie the spatial relationship between resting state aerobic glycolysis and amyloid deposition in AD.

We have previously demonstrated that ISF Aβ levels exhibit diurnal fluctuation - ISF Aβ concentration is significantly greater during waking conditions compared to sleep[26]. Given that neuronal activity directly regulates ISF Aβ levels, we reasoned that diurnal fluctuation of neuronal activity may contribute to diurnal fluctuation of ISF Aβ. Indeed, previous data suggest that periods of wakefulness are associated with net synaptic potentiation and periods of sleep are associated with synaptic downscaling and depression[28]. Here we show that ISF lactate concentration exhibits diurnal fluctuation and is closely associated with the diurnal fluctuation of ISF Aβ. These results are consistent with the notion that fluctuation of neuronal activity levels during the sleep/wake cycle contributes to the diurnal fluctuation of ISF Aβ levels in vivo. This observation further supports the hypothesis that physiological neuronal activity dynamically regulates ISF Aβ levels in vivo.

More generally, our results suggest that factors that elevate endogenous neuronal activity over prolonged periods may accelerate progression of Aβ deposition. In support of this hypothesis, recent fMRI data suggests that cognitively normal *APOE* ε4 carriers exhibit elevated resting state activity in the default network and increased hippocampal activation during a memory encoding task compared to non-carriers[43]. Thus, in addition to apoE isoform-dependent differences in apoE-Aβ interactions[44], elevated lifetime neuronal activity may be a complementary mechanism by which ε4 expression increases AD risk. Conversely, factors that reduce activity in vulnerable neural networks may slow the progression of β-amyloidosis and reduce AD risk. For example, epidemiological evidence suggests that educational attainment is negatively correlated with AD risk[45]. As default network activity is suppressed during cognitively demanding tasks, one possibility is that education reduces AD risk by reducing neuronal activity and Aβ generation within the default network.

It is noteworthy that the regional distribution of lesions in mouse models of glutamate-induced excitotoxicity is strikingly similar to the distribution of Aβ deposition described herein[46]. As neuronal activity regulates both Aβ and glutamate release at the synapse, the presently described regional differences in basal neuronal activity may also underlie the distribution of glutamate-induced excitotoxic lesions. A more detailed understanding of the regional distribution of pre- and post-synaptic elements may provide insight regarding the structural basis of neuronal activity patterns in normal brain and how patterns of neuronal/synaptic activity might contribute to a variety of neurological lesions.

METHODS

Mice

Male and female Tg2576$^{+/-19}$ (gift of Karen Ashe, Univ. of Minnesota) x B6SJL mice (Taconic Farms) were aged to 17.5 ± 0.5 months of age for Aβ immunohistochemistry and X-34 staining experiments and 3.5 ± 0.5 months of age for all other experiments. Male and female wild-type (B6SJL) mice were utilized at 5.5 ± 0.5 months of age. Male and female APPswe/PS1ΔE9 x B6C3 (APP/PS1; The Jackson Laboratory) were utilized at 7–7.5 months of age. When two or more groups of animals were compared, groups were sex-matched. Animals were given ad libitum access to food and water. All experimental protocols were approved by the Animal Studies Committee at Washington University.

Plaque deposition analyses

Brain tissue was dissected and flash-frozen for 1 minute in isopentane chilled with dry ice before sectioning on a cryostat (Leica). Serial coronal sections (30 μm section thickness) were collected from the genu of the corpus callosum to caudal hippocampus. Sections (each separated by 180 μm) were stained with biotinylated 3D6 antibody (anti $Aβ_{1–5}$; generous gift from Eli Lilly) to visualize Aβ immunopositive plaques or X-34 dye to visualize fibrillar amyloid plaques. Immunostained sections were scanned using a NanoZoomer slide scanner (Hamamatsu Photonics). X-34-stained sections were imaged using a fluorescence microscope (Nikon) and images were captured using a digital CCD color camera (QCapture Pro version 6.0, QImaging). Quantitative analysis of percent area covered by immuno- or X-34-positive staining was performed as described previously[47]. Briefly, images of immunostained sections were exported with NDP viewer software (Hamamatsu Photonics), converted to 8-bit grayscale using ACDSee Pro 2 software (ACD Systems), thresholded to highlight Aβ-specific staining and analyzed using ImageJ software (National Institutes of Health). Images of X-34-stained sections were converted to 16-bit grayscale, thresholded to highlight X-34-specific staining and analyzed using ImageJ software. A mouse brain atlas[48] was used to identify piriform cortex, cingulate cortex, barrel cortex, hippocampus and striatum for quantitative analysis of immuno- and X-34-positive staining.

In vivo microdialysis

In vivo microdialysis used to measure Aβ in the brain ISF of awake, freely behaving mice was performed essentially as described[2]. Briefly, guide cannulae (BR-style, Bioanalytical Systems) were stereotaxically implanted into piriform cortex (bregma + 1.0 mm, 3.8 mm lateral to midline, 1.2 mm below the dura at a 21° angle), barrel cortex (at bregma, 2.0 mm lateral to midline, 1.0 mm below the dura at a 32° angle), hippocampus (bregma 3.1 mm, 2.5 mm lateral to midline, 1.2 mm below the dura at a 12° angle) or striatum (bregma + 0.5 mm, 1.8 mm lateral to midline, 1.4 mm below the dura at a 0° angle) for determination of steady-state Aβ and lactate levels. For vibrissae removal and stimulation experiments, guide cannulae were implanted into posterior barrel cortex (bregma – 1.5 mm, 1.7 mm lateral to midline, 0.7 mm below the dura at a 49° angle). Probe placement in the region of interest was verified by cresyl violet staining. Microdialysis probes (2 mm; 38 kDa molecular weight cut-off; BR-style, BioAnalytical Systems) were connected to a syringe pump (Stoelting Co.) and artificial cerebrospinal fluid (pH 7.35) containing (in mM) 1.3 $CaCl_2$,

1.2 $MgSO_4$, 3 KCl, 0.4 KH_2PO_4, 25 $NaHCO_3$, and 122 NaCl was continuously perfused through the microdialysis probe at a constant flow rate. For measurement of $A\beta_{x-40}$, $A\beta_{1-x}$, and lactate in Tg2576 mice, a flow rate of 1.0 μl min^{-1} was used. For measurement of $A\beta_{x-42}$ in Tg2576 mice, a flow rate of 0.3 μl min^{-1} was used. For measurement of $A\beta_{x-40}$ and lactate in wild-type (B6SJL) mice, a flow rate of 0.5 μl min^{-1} was used. For PTX and TTX infusion via reverse microdialysis into hippocampus of young Tg2576 mice, a stable baseline of ISF $A\beta_{x-40}$ and lactate levels was obtained before drug treatment began. PTX (12.5 μM) was continuously infused for 12 h. Following a 5 h washout period, TTX (5 μM) was continuously infused for 16 h before concluding the experiment. For ISF Aβ half-life experiments, a stable baseline of ISF $A\beta_{x-40}$ was obtained before intraperitoneally injecting each mouse with 10 mg kg^{-1} of the γ-secretase inhibitor Compound E (Custom synthesis, AsisChem Inc.). The plot of the common logarithm of percent baseline ISF $A\beta_{x-40}$ concentration versus time after injection was linear in each region, suggesting first-order kinetics. Therefore, the elimination half-life of ISF $A\beta_{x-40}$ in each mouse was calculated using the slope of the linear regression from log(percent baseline ISF $A\beta_{x-40}$) versus time as described previously[2]. In vibrissae removal experiments, stable baseline levels of ISF $A\beta_{x-40}$ and ISF lactate were obtained before all mystacial vibrissae contralateral to the microdialysis probe were trimmed to within 1 mm of the facial pad using fine surgical scissors (Roboz). Vibrissae ipsilateral to the microdialysis probe remained intact throughout the experiment. In vibrissae stimulation experiments, mice were anesthetized with ketamine-xylazine (130.4 and 20.1 mg kg^{-1}, respectively) during the microdialysis sampling period. All vibrissae ipsilateral to the microdialysis probe were trimmed to within 1 mm of the facial pad using fine surgical scissors (Roboz). Mechanical vibrissae stimulation was performed by gently brushing vibrissae contralateral to the microdialysis probe using a cotton-tipped applicator for 30 min (5–7 Hz, 4 s burst, 4 s inter-burst interval). In sleep/wake experiments, guide cannulae were implanted into hippocampus 2 weeks before microdialysis began. Mice were habituated to the microdialysis sampling environment for 3 days and microdialysis samples collected during this period were discarded. On the 4^{th} day, samples were collected and stored for analysis.

ELISA

Microdialysis samples were analyzed for $A\beta_{x-40}$, $A\beta_{x-42}$, or $A\beta_{1-x}$ using species-specific sandwich ELISAs. Briefly, $A\beta_{x-40}$, $A\beta_{x-42}$, and $A\beta_{1-x}$ were captured using monoclonal antibodies targeted against amino acids 35–40 (HJ2), 37–42 (HJ7.4) and 13–28 (m266) of Aβ, respectively. For $A\beta_{x-40}$ and $A\beta_{x-42}$ assays, a biotinylated central domain monoclonal antibody (HJ5.1) followed by streptavidin-poly-HRP-40 (Fitzgerald) was used to detect. For $A\beta_{1-x}$ assays, a biotinylated N-terminal domain monoclonal antibody (3D6B) followed by streptavidin-poly-HRP-20 was used to detect (Fitzgerald). The antibodies m266 and 3D6B were generous gifts from Eli Lilly. All assays were developed using Super Slow ELISA TMB (Sigma) and read on a Bio-Tek Synergy 2 plate reader at 650 nm.

Intraparenchymal EEG recording

Depth EEG recording was performed as previously described[17]. Briefly, bipolar recording electrodes (A-M Systems) were affixed to the microdialysis guide cannula and stereotaxically implanted into hippocampus. Electrodes extended approximately 1 mm from

the tip of the guide cannula to position the electrodes near the center of the 2 mm microdialysis membrane. EEG activity was assessed using a P511K A.C. Pre-amplifier (Grass Instruments), digitized with a DigiData 1440A Data Acquisition System (Molecular Devices), and recorded digitally using pClamp 10.2 (Molecular Devices).

Lactate assay

An enzymatic lactate assay kit (BioVision) was utilized to measure lactate present in ISF samples according to the manufacturer's instructions. Assays were read on a Bio-Tek Synergy 2 plate reader at 570 nm.

Western blot

Dissected tissue from piriform, barrel and cingulate cortices was homogenized in radioimmunoprecipitation assay (RIPA) buffer [150 mM NaCl, 50 mM Tris, 0.5% deoxycholic acid, 1% Triton X-100, 0.1% SDS, 2.5 mM EDTA and a protease inhibitor cocktail (Calbiochem; pH 8.0; 10 μl mg^{-1} tissue wet weight)] by manual wand homogenization. Dissected tissue from hippocampus and striatum was homogenized in RIPA buffer by sonication. Tissue homogenates were centrifuged at 12,000 rpm at 4°C for 15 min and supernatant was saved for analysis. In addition to normalizing Western blot results to equal amounts of brain wet weight loaded per lane, a loading control was also performed for each tissue sample. Equal volumes of tissue samples were spiked with 5 μg fluorescein-conjugated bovine serum albumin (Biosearch Technologies) to serve as a loading control and equal volumes of tissue homogenate were separated by 4–12% Bis-Tris gel electrophoresis (Invitrogen) under reducing conditions. Nitrocellulose blots (0.2 μm probe size, BioRad) were probed for full-length APP using 6E10 antibody (human-specific; Covance) or APP CTFs using CT695 antibody (reactivity with human and mouse; Invitrogen). Normalized band intensity was quantified using ImageJ (National Institutes of Health).

Sleep/wake monitoring

Polysomnographic sleep-wake cycle analysis of mice was performed as described previously[26]. Briefly, electroencephalograph (EEG) and electromyogram (EMG) electrodes were implanted simultaneously with the microdialysis guide cannula. For EEG recording, two stainless steel screws attached to wire electrodes were placed over the right frontal bone (bregma +1.0 mm, 1.5 mm lateral to midline) and the right parietal bone (bregma −3.0 mm, 2.5 mm lateral to midline). Two wire electrodes were directly inserted into the neck musculature for EMG recording. The ground electrode was placed on the skull over the cerebellum. Insulated leads from the EEG and EMG electrodes were soldered to a mini-connector. After surgery, mice were housed in 12 hour light/12 hour dark conditions (light phase began at 6 a.m.) for 2 weeks before recording began. To monitor the sleep-wake cycle, mice were transferred to recording cages maintained in 12 hour light/12 hour dark conditions (light phase began at 6 a.m.) and the mini-connector was connected to flexible recording cables. Mice were habituated to the recording cages for 3 days. At the conclusion of the habituation period, EEG and EMG recording began simultaneously with microdialysis sample collection. EEG and EMG signals were displayed on a monitor and stored in a computer for off-line analysis of sleep states. EEG and EMG recordings were assessed using

a P511K A.C. Pre-amplifier (Grass-Telefactor Instruments), digitized with a DigiData 1440A Data Acquisition System (Molecular Devices), and recorded digitally using pClamp 10.2 (Molecular Devices). EEG and EMG signals were filtered (EEG: high pass 1 Hz; low pass 30 Hz; EMG: high pass 10 Hz; low pass 100 Hz) and used to identify vigilance states. EEG and EMG recordings were scored semiautomatically using sleep scoring software (SleepSign, Kissei Comtec Co., LTD., Japan) and binned into 10-s epochs as wakefulness, rapid eye movement (REM) sleep, and non-REM (NREM) sleep per standard criteria of rodent sleep. Semiautomatic sleep scoring was visually inspected and corrected when appropriate.

Thinned-skull cranial window surgery

Thinned-skull cranial windows were prepared on the day of the first multiphoton imaging session as described previously[4]. Briefly, mice were anesthetized under volatile isoflurane and the skin and periosteum were removed to expose the skull. A high-speed drill and microsurgical blade (Surgistar) were used to thin the skull until the skull was transparent and displayed flexibility. One cranial window (2×2 mm) was prepared over barrel cortex (bregma – 1.5 mm, 3.5 mm lateral to midline) of each hemisphere.

In vivo multiphoton microscopy

Longitudinal multiphoton microscopy to monitor amyloid plaque growth was performed as described previously[4]. Briefly, mice were injected intraperitoneally with the fluorescent amyloid-binding compound methoxy-X04[49] (5 mg ml^{-1}) 24 hours prior to each multiphoton imaging session. Animals were mounted on a custom-built stereotaxic apparatus and a small ring of molten bone wax was applied to the skull surrounding the perimeter of the window to create a water immersion chamber. The cranial window was centered under the objective lens on a two-photon microscope [LSM 510 META NLO system (Carl Zeiss Inc.) with a Cameleon Ti:Sapphire laser (Coherent Inc.)]. Two-photon fluorescence was generated with 750 nm excitation and fluorescence emission was detected at 435–485 nm. A 10X water-immersion objective [numerical aperture (NA) = 0.33, Zeiss] was used to create a site map during initial imaging and a 40X water-immersion objective (NA = 0.75, Zeiss) was used for high-resolution quantification of individual amyloid plaques. Incremental *z*-stack image series (step distance = 10 and 5 μm under 10X and 40X objectives, respectively) were acquired from the skull surface to approximately 200 μm into cortex. To determine the effect of long-term vibrissae deprivation on amyloid plaque formation and growth, the same sites of each hemisphere of barrel cortex in each animal were imaged on day 0 and day 28. Collapsed *z*-stack images of each amyloid plaque were measured by cross-sectional area using SigmaScan Pro Image Analysis Software (Systat Software) as previously described[4]. Plaques were excluded from analysis if they were located at the edge of the window, exhibited fluorescence intensity less than the mean intensity of an adjacent background region or if the image acquisition was affected by motion artifacts from heartbeat or respiration.

Double immunofluorescence

To compare astrocytic and microglia activation in barrel cortex following long-term vibrissae deprivation, animals were transcardiallyperfused with 0.9% saline followed by 4% paraformaldehyde (PFA) in 0.01 M PBS immediately following the final multiphoton imagingsession. Brains were removed and postfixed in 4% PFAfor an additional 4 h. Coronal free-floating sections (50 μm thick)were cut on a cryostat (Leica). Sections were incubated overnight at4°C in a combination of mouse anti-GFAP monoclonal antibody (Sigma) and rabbit anti-Iba1 (Wako Chemicals). A secondaryantibody mixture of Alexa Fluor 488-conjugateddonkey anti-mouse IgG (Invitrogen) and Cy3-conjugated donkey anti-rabbit IgG (Jackson ImmunoResearch Laboratories) was used to detect. Sectionswere imaged using a confocal microscope(Zeiss LSM).

Statistical analysis

Statistical significance was determined by two-tailed t-test if 2 groups were compared. When variance differed significantly between groups, Welch's t-test was used. One-way ANOVA followed by Tukey's post hoc test for multiple comparisons tests were used when greater than 2 groups were compared. Correlation was determined using Pearson product moment correlation test. All statistical analyses were performed using Prism version 4.0 for Windows (GraphPad). Values were accepted as significant if $P < 0.05$.

Supplementary Material

Refer to Web version on PubMed Central for supplementary material.

Acknowledgments

This work was supported by NIH grants AG033452 (A.W.B.), AG029524 (J.R.C.), AG568127 (J.R.C.), NS06833 (M.E.R.), NS67905 (J-M.L.), NS32636 (J-M.L.), AG13956 (D.M.H.), P30NS057105 (D.M.H.) and the Cure Alzheimer's Fund (D.M.H.). We thank Dr. Robert H. Mach (Washington University School of Medicine, St. Louis) for generously providing methoxy-X04 and X-34. We thank Eli Lilly and Co. for generously providing m266 and biotinylated 3D6 anti Aβ antibodies.

References

1. Selkoe DJ. Alzheimer's disease: genes, proteins, and therapy. Physiol Rev. 2001; 81:741–766. [PubMed: 11274343]
2. Cirrito JR, et al. In vivo assessment of brain interstitial fluid with microdialysis reveals plaque-associated changes in amyloid-beta metabolism and half-life. J Neurosci. 2003; 23:8844–8853. [PubMed: 14523085]
3. Meyer-Luehmann M, et al. Extracellular amyloid formation and associated pathology in neural grafts. Nat Neurosci. 2003; 6:370–377. [PubMed: 12598899]
4. Yan P, et al. Characterizing the appearance and growth of amyloid plaques in APP/PS1 mice. J Neurosci. 2009; 29:10706–10714. [PubMed: 19710322]
5. Raichle ME, et al. A default mode of brain function. Proc Natl Acad Sci U S A. 2001; 98:676–682. [PubMed: 11209064]
6. Buckner RL, et al. Molecular, structural, and functional characterization of Alzheimer's disease: evidence for a relationship between default activity, amyloid, and memory. J Neurosci. 2005; 25:7709–7717. [PubMed: 16120771]
7. Buckner RL, Andrews-Hanna JR, Schacter DL. The brain's default network: anatomy, function, and relevance to disease. Ann N Y Acad Sci. 2008; 1124:1–38. [PubMed: 18400922]

8. Buckner RL, et al. Cortical hubs revealed by intrinsic functional connectivity: mapping, assessment of stability, and relation to Alzheimer's disease. J Neurosci. 2009; 29:1860–1873. [PubMed: 19211893]
9. Vaishnavi SN, et al. Regional aerobic glycolysis in the human brain. Proc Natl Acad Sci U S A. 2010; 107:17757–17762. [PubMed: 20837536]
10. Vlassenko AG, et al. Spatial correlation between brain aerobic glycolysis and amyloid-beta (Abeta) deposition. Proc Natl Acad Sci U S A. 2010; 107:17763–17767. [PubMed: 20837517]
11. Greicius MD, Srivastava G, Reiss AL, Menon V. Default-mode network activity distinguishes Alzheimer's disease from healthy aging: evidence from functional MRI. Proc Natl Acad Sci U S A. 2004; 101:4637–4642. [PubMed: 15070770]
12. Hedden T, et al. Disruption of functional connectivity in clinically normal older adults harboring amyloid burden. J Neurosci. 2009; 29:12686–12694. [PubMed: 19812343]
13. Sperling RA, et al. Amyloid deposition is associated with impaired default network function in older persons without dementia. Neuron. 2009; 63:178–188. [PubMed: 19640477]
14. Hyder F, et al. Neuronal-glial glucose oxidation and glutamatergic-GABAergic function. J Cereb Blood Flow Metab. 2006; 26:865–877. [PubMed: 16407855]
15. Kamenetz F, et al. APP processing and synaptic function. Neuron. 2003; 37:925–937. [PubMed: 12670422]
16. Wei W, et al. Amyloid beta from axons and dendrites reduces local spine number and plasticity. Nat Neurosci. 2010; 13:190–196. [PubMed: 20037574]
17. Cirrito JR, et al. Synaptic activity regulates interstitial fluid amyloid-beta levels in vivo. Neuron. 2005; 48:913–922. [PubMed: 16364896]
18. Cirrito JR, et al. Endocytosis is required for synaptic activity-dependent release of amyloid-beta in vivo. Neuron. 2008; 58:42–51. [PubMed: 18400162]
19. Hsiao K, et al. Correlative memory deficits, Abeta elevation, and amyloid plaques in transgenic mice. Science. 1996; 274:99–102. [PubMed: 8810256]
20. Pellerin L, Magistretti PJ. Glutamate uptake into astrocytes stimulates aerobic glycolysis: a mechanism coupling neuronal activity to glucose utilization. Proc Natl Acad Sci U S A. 1994; 91:10625–10629. [PubMed: 7938003]
21. Uehara T, Sumiyoshi T, Itoh H, Kurata K. Lactate production and neurotransmitters; evidence from microdialysis studies. Pharmacol Biochem Behav. 2008; 90:273–281. [PubMed: 18502489]
22. Woolsey TA, Van der Loos H. The structural organization of layer IV in the somatosensory region (SI) of mouse cerebral cortex. The description of a cortical field composed of discrete cytoarchitectonic units. Brain Res. 1970; 17:205–242. [PubMed: 4904874]
23. Melzer P, et al. A magnetic device to stimulate selected whiskers of freely moving or restrained small rodents: its application in a deoxyglucose study. Brain Res. 1985; 348:229–240. [PubMed: 4075083]
24. Durham D, Woolsey TA. Acute whisker removal reduces neuronal activity in barrels of mouse SmL cortex. J Comp Neurol. 1978; 178:629–644. [PubMed: 632373]
25. Rojas MJ, Navas JA, Rector DM. Evoked response potential markers for anesthetic and behavioral states. Am J Physiol Regul Integr Comp Physiol. 2006; 291:R189–196. [PubMed: 16455771]
26. Kang JE, et al. Amyloid-beta dynamics are regulated by orexin and the sleep-wake cycle. Science. 2009; 326:1005–1007. [PubMed: 19779148]
27. Riedner BA, et al. Sleep homeostasis and cortical synchronization: III. A high-density EEG study of sleep slow waves in humans. Sleep. 2007; 30:1643–1657. [PubMed: 18246974]
28. Vyazovskiy VV, Cirelli C, Pfister-Genskow M, Faraguna U, Tononi G. Molecular and electrophysiological evidence for net synaptic potentiation in wake and depression in sleep. Nat Neurosci. 2008; 11:200–208. [PubMed: 18204445]
29. Gilestro GF, Tononi G, Cirelli C. Widespread changes in synaptic markers as a function of sleep and wakefulness in Drosophila. Science. 2009; 324:109–112. [PubMed: 19342593]
30. Jankowsky JL, et al. Mutant presenilins specifically elevate the levels of the 42 residue beta-amyloid peptide in vivo: evidence for augmentation of a 42-specific gamma secretase. Hum Mol Genet. 2004; 13:159–170. [PubMed: 14645205]

31. Bahmanyar S, et al. Localization of amyloid beta protein messenger RNA in brains from patients with Alzheimer's disease. Science. 1987; 237:77–80. [PubMed: 3299701]
32. Goedert M. Neuronal localization of amyloid beta protein precursor mRNA in normal human brain and in Alzheimer's disease. EMBO J. 1987; 6:3627–3632. [PubMed: 3322812]
33. Vassar R, et al. Beta-secretase cleavage of Alzheimer's amyloid precursor protein by the transmembrane aspartic protease BACE. Science. 1999; 286:735–741. [PubMed: 10531052]
34. Page K, Hollister R, Tanzi RE, Hyman BT. In situ hybridization analysis of presenilin 1 mRNA in Alzheimer disease and in lesioned rat brain. Proc Natl Acad Sci U S A. 1996; 93:14020–14024. [PubMed: 8943053]
35. Irizarry MC, McNamara M, Fedorchak K, Hsiao K, Hyman BT. APPSw transgenic mice develop age-related A beta deposits and neuropil abnormalities, but no neuronal loss in CA1. J Neuropathol Exp Neurol. 1997; 56:965–973. [PubMed: 9291938]
36. Irizarry MC, Locascio JJ, Hyman BT. beta-site APP cleaving enzyme mRNA expression in APP transgenic mice: anatomical overlap with transgene expression and static levels with aging. Am J Pathol. 2001; 158:173–177. [PubMed: 11141490]
37. Bigl M, et al. Expression of beta-secretase mRNA in transgenic Tg2576 mouse brain with Alzheimer plaque pathology. Neurosci Lett. 2000; 292:107–110. [PubMed: 10998560]
38. Goldstein ME, et al. Ex vivo occupancy of gamma-secretase inhibitors correlates with brain beta-amyloid peptide reduction in Tg2576 mice. J Pharmacol Exp Ther. 2007; 323:102–108. [PubMed: 17640949]
39. Meyer-Luehmann M, et al. Exogenous induction of cerebral beta-amyloidogenesis is governed by agent and host. Science. 2006; 313:1781–1784. [PubMed: 16990547]
40. Eisele YS, et al. Peripherally applied Abeta-containing inoculates induce cerebral beta-amyloidosis. Science. 2010; 330:980–982. [PubMed: 20966215]
41. Harris JA, et al. Transsynaptic progression of amyloid-beta-induced neuronal dysfunction within the entorhinal-hippocampal network. Neuron. 2010; 68:428–441. [PubMed: 21040845]
42. Lazarov O, Lee M, Peterson DA, Sisodia SS. Evidence that synaptically released beta-amyloid accumulates as extracellular deposits in the hippocampus of transgenic mice. J Neurosci. 2002; 22:9785–9793. [PubMed: 12427834]
43. Filippini N, et al. Distinct patterns of brain activity in young carriers of the APOE-epsilon4 allele. Proc Natl Acad Sci U S A. 2009; 106:7209–7214. [PubMed: 19357304]
44. Kim J, Basak JM, Holtzman DM. The role of apolipoprotein E in Alzheimer's disease. Neuron. 2009; 63:287–303. [PubMed: 19679070]
45. Flicker L. Modifiable lifestyle risk factors for Alzheimer's disease. J Alzheimers Dis. 2010; 20:803–811. [PubMed: 20182016]
46. Olney JW, Wozniak DF, Farber NB. Excitotoxic neurodegeneration in Alzheimer disease. New hypothesis and new therapeutic strategies. Arch Neurol. 1997; 54:1234–1240. [PubMed: 9341569]
47. Kim J, et al. Overexpression of low-density lipoprotein receptor in the brain markedly inhibits amyloid deposition and increases extracellular A beta clearance. Neuron. 2009; 64:632–644. [PubMed: 20005821]
48. Franklin, KB.; Paxinos, G. The Mouse Brain in Stereotaxic Coordinates. Academic Press; San Diego: 1996.
49. Klunk WE, et al. Imaging Abeta plaques in living transgenic mice with multiphoton microscopy and methoxy-X04, a systemically administered Congo red derivative. J Neuropathol Exp Neurol. 2002; 61:797–805. [PubMed: 12230326]

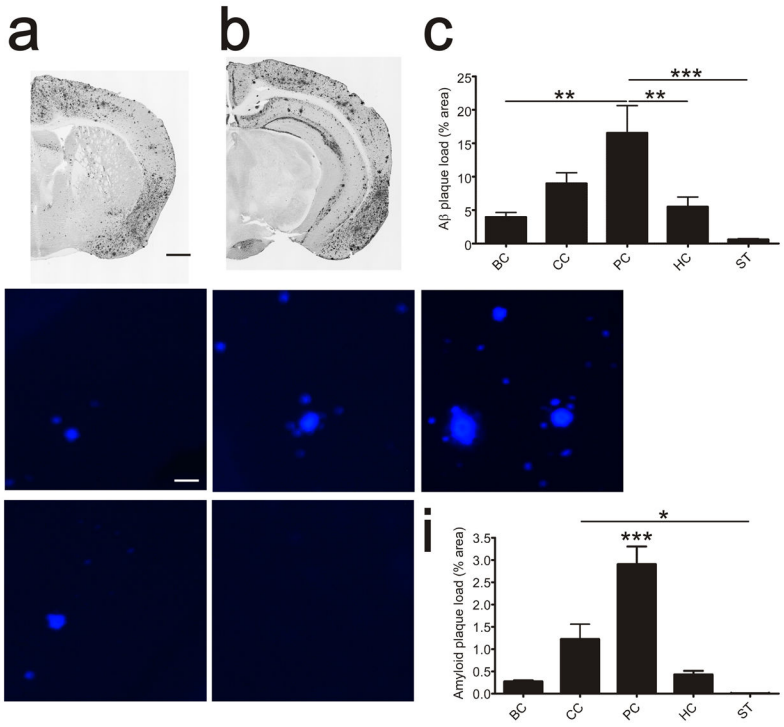

Figure 1.

Distribution of Aβ and amyloid plaque deposition in Tg2576 mouse brain. (**a**,**b**) Representative brain sections from aged (17.5 ± 0.5 months old) Tg2576 mice stained with biotinylated-3D6 antibody (anti $A\beta_{1-5}$) to visualize Aβ immunopositive plaques (n = 7 per group). Scale bar, 750 μM. (**c**) A stepwise increase in percent brain area occupied by Aβ deposition was present across barrel (BC), cingulate (CC) and piriform (PC) cortices. Aβ plaque burden in hippocampus (HC) was similar to barrel cortex while striatum (ST) exhibited the lowest level of plaque deposition of all regions examined (one-way ANOVA, Tukey's post hoc test for multiple comparisons). (**d**–**h**) Representative images of barrel cortex (**d**), cingulate cortex (**e**), piriform cortex (**f**), hippocampus (**g**) and striatum (**h**) of aged Tg2576 mice stained with the amyloid binding dye, X-34 (n = 6 per group). Scale bar, 50 μM. (**i**) Percent area occupied by X-34 positive amyloid deposition was greater in piriform cortex compared to all other brain regions examined. A stepwise increase in amyloid deposition was present across barrel, cingulate and piriform cortices. Amyloid plaque burden in hippocampus was similar to barrel cortex while X-34 positive staining was not detected in striatum (one-way ANOVA, Tukey's post hoc test for multiple comparisons). **, $P < 0.01$; ***, $P < 0.001$. Values represent mean ± SEM.

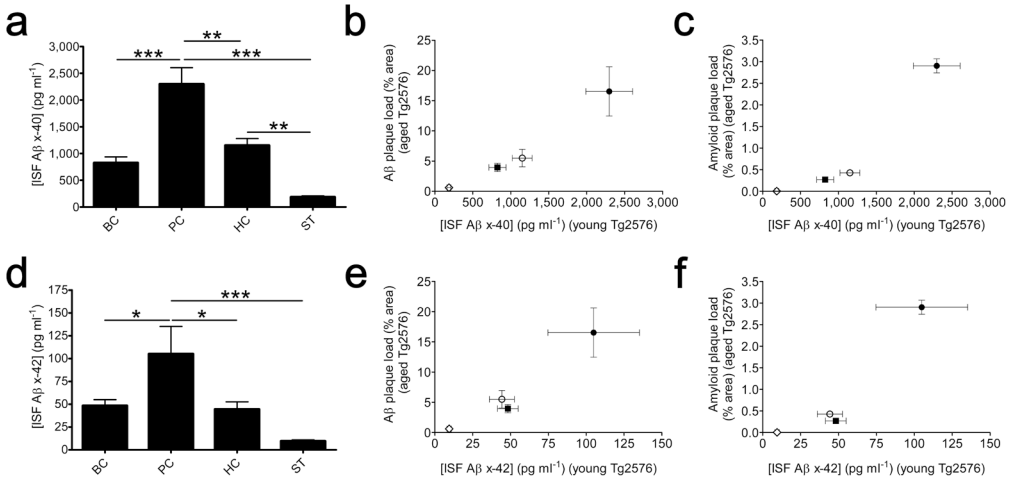

Figure 2.

Steady-state ISF Aβ levels in young Tg2576 mice prior to plaque deposition are associated with the level of region-specific plaque deposition in aged Tg2576 mice. (**a**) In vivo microdialysis was performed to measure the steady-state concentration of ISF $A\beta_{x\text{-}40}$ in barrel cortex (BC), piriform cortex (PC), hippocampus (HC) and striatum (ST) of 3.5 ± 0.5 month-old Tg2576 mice prior to the onset of plaque deposition (n = 5–6 per group; one-way ANOVA, Tukey's post hoc test for multiple comparisons). Steady-state levels of ISF $A\beta_{x\text{-}40}$ measured in each brain region of young Tg2576 mice were closely associated with the level of subsequent Aβ (**b**) and amyloid (**c**) plaque deposition in each brain region of aged Tg2576 mice. (**d**) In vivo microdialysis was performed to measure the steady-state concentration of ISF $A\beta_{x\text{-}42}$ in barrel cortex, piriform cortex, hippocampus and striatum of 3.5 ± 0.5 month-old Tg2576 mice prior to the onset of plaque deposition (n = 5–8 per group; one-way ANOVA, Tukey's post hoc test for multiple comparisons). Steady-state levels of ISF $A\beta_{x\text{-}42}$ measured in each brain region of young Tg2576 mice were closely associated with the level of subsequent Aβ (**e**) and amyloid (**f**) plaque deposition in each brain region of aged Tg2576 mice. ◇, striatum; ■, barrel cortex, ○, hippocampus; ●, piriform cortex. *, $P < 0.05$; **, $P < 0.01$; ***, $P < 0.001$. Values represent mean ± SEM.

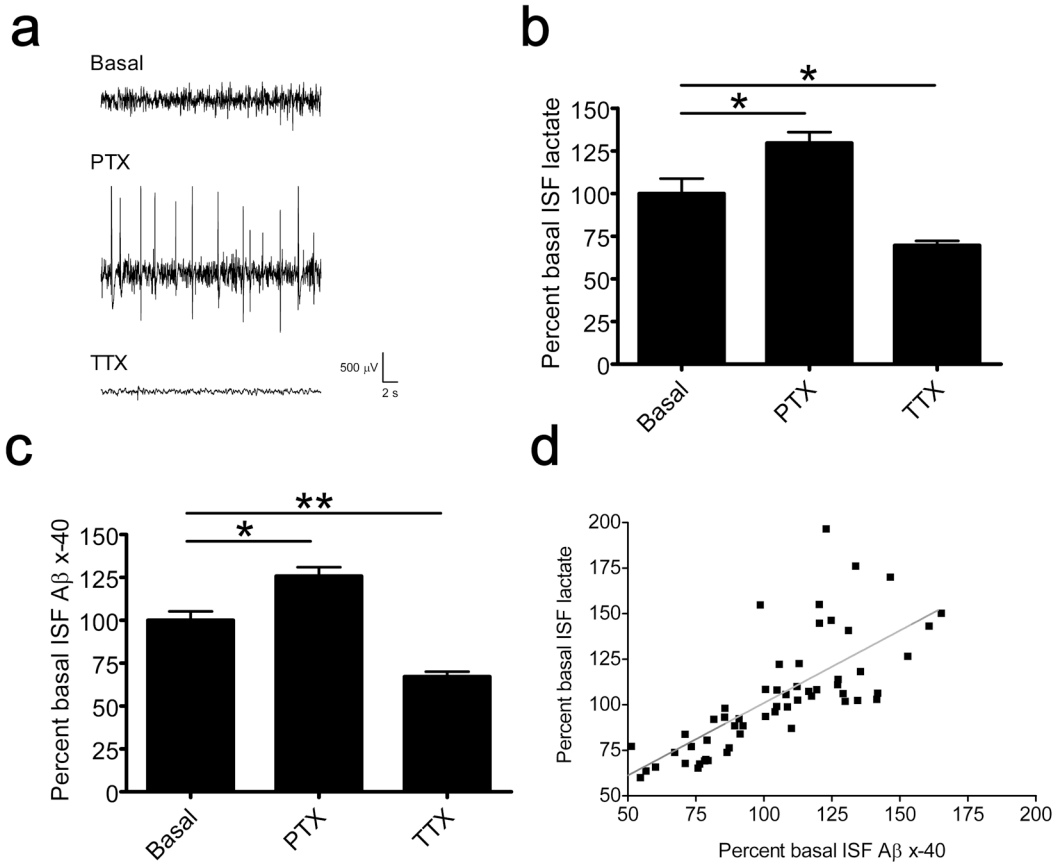

Figure 3.

Neuronal activity regulates ISF lactate concentration in vivo. (**a**) Representative intraparenchymal EEG recordings from hippocampus of young Tg2576 mice during basal conditions, picrotoxin (PTX; 12.5 μM) treatment or tetrodotoxin (TTX; 5 μM) treatment via in vivo microdialysis (n = 4 per group). (**b**) Local PTX infusion increased ISF lactate levels and local TTX infusion decreased ISF lactate levels in hippocampus of young Tg2576 mice (n = 4 per group; two-tailed t-test). (**c**) Local PTX infusion increased ISF $A\beta_{x\text{-}40}$ levels and local TTX infusion decreased ISF $A\beta_{x\text{-}40}$ levels in hippocampus of young Tg2576 mice (n = 4 per group; two-tailed t-test). Values in **b**,**c** represent analyte levels during the final 6 hours of drug treatment. (**d**) ISF lactate levels were correlated with ISF $A\beta_{x\text{-}40}$ levels across treatment periods (Pearson r = 0.7645; $P < 0.0001$). *, $P < 0.05$; **, $P < 0.01$. Values represent mean ± SEM.

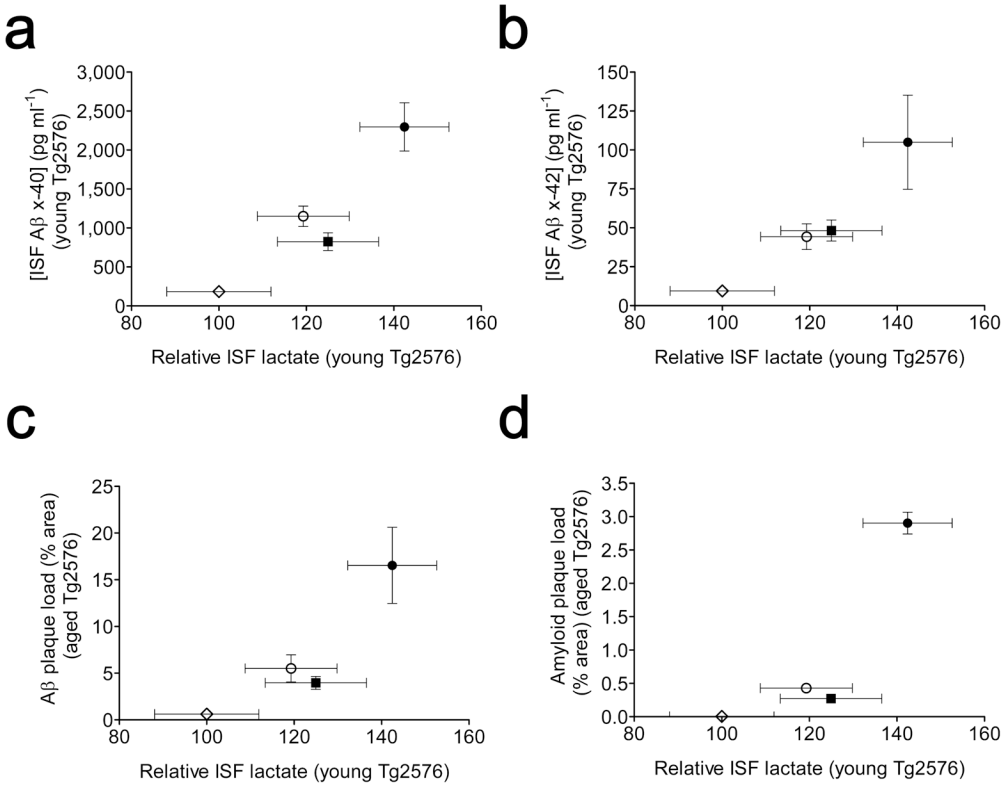

Figure 4.

Steady-state ISF lactate levels in young Tg2576 mice are closely associated with regional ISF Aβ levels in young Tg2576 mice and plaque deposition in aged Tg2576 mice. (**a–d**) In vivo microdialysis was performed to measure steady-state ISF lactate levels in barrel cortex, piriform cortex, hippocampus and striatum of young Tg2576 mice (n = 6–7 per group). ISF lactate level in each brain region was closely associated with the concentration of ISF $A\beta_{x\text{-}40}$ (**a**) and ISF $A\beta_{x\text{-}42}$ (**b**) in each brain region of young Tg2576 mice. ISF lactate level in each brain region of young Tg2576 mice was also closely associated with the level of Aβ (**c**) and amyloid (**d**) plaque deposition in each brain region of aged Tg2576 mice. ◇, striatum; ■, barrel cortex, ○, hippocampus; ●, piriform cortex. Values represent mean ± SEM.

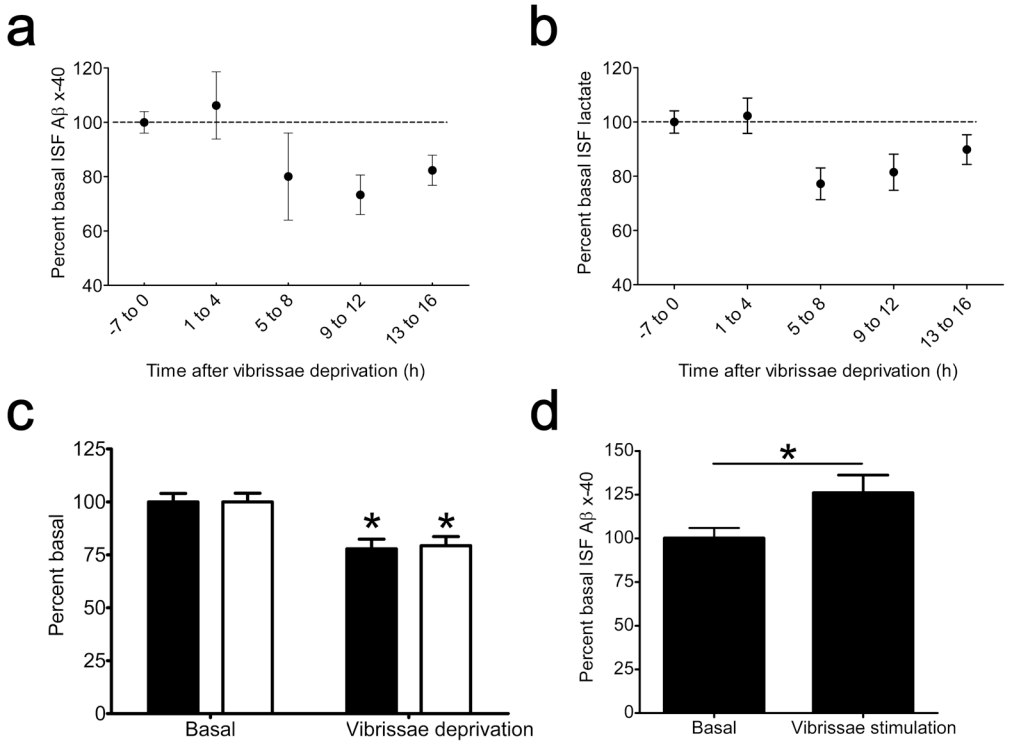

Figure 5.

Vibrissal activity regulates ISF Aβ levels in vivo. (**a**–**c**) In vivo microdialysis was performed in posterior barrel cortex of young Tg2576 mice. After establishing stable basal ISF $A\beta_{x\text{-}40}$ and lactate levels, all vibrissae contralateral to the microdialysis probe were trimmed to within 1 mm of the facial pad and microdialysis sample collection continued for 16 hr to determine the effect of vibrissae deprivation on ISF $A\beta_{x\text{-}40}$ and lactate levels in barrel cortex. Vibrissae deprivation decreased ISF $A\beta_{x\text{-}40}$ (**a**, ■ in **c**) and lactate (**b**, □ in **c**) levels relative to baseline (n = 6–7; two-tailed t-test). (**d**) In vivo microdialysis was performed in barrel cortex in a separate cohort of young Tg2576 mice that underwent subsequent unilateral vibrissae stimulation. Baseline $A\beta_{x\text{-}40}$ values were obtained for a 30 minute period. Unilateral mechanical stimulation of vibrissae contralateral to the microdialysis probe (5–7 Hz, 4 s burst, 4 s inter-burst interval) was performed for 30 minutes. Vibrissae stimulation increased ISF $A\beta_{x\text{-}40}$ levels compared to control conditions (n = 4; two-tailed t-test). *, $P < 0.05$; **, $P < 0.01$. Values represent mean ± SEM.

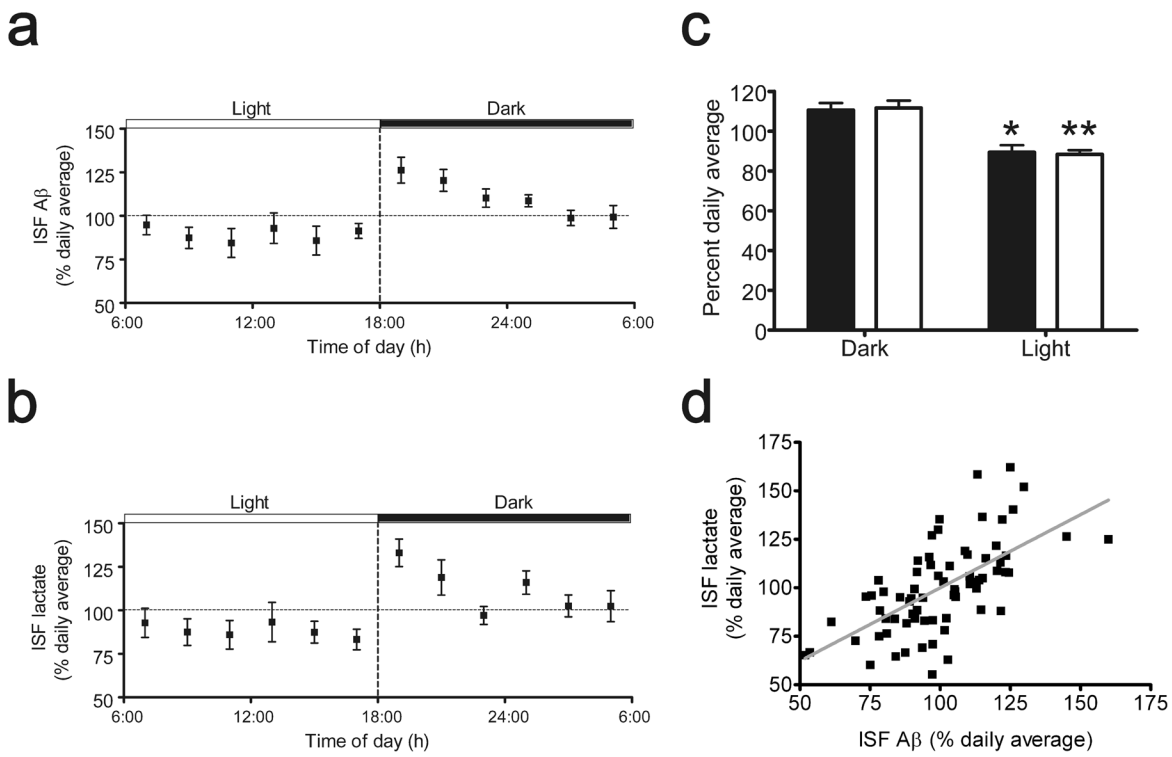

Figure 6.

Diurnal fluctuation of ISF Aβ is closely associated with ISF lactate levels. (**a**–**c**) In vivo microdialysis was performed in hippocampus of young Tg2576 mice housed in 12 hour light/12 hour dark conditions. ISF $A\beta_{1\text{-}x}$ levels exhibited diurnal fluctuation (**a**) and were significantly greater in the dark period compared to the light period (■ in **c**; $n = 6$; two-tailed t-test). ISF lactate levels also exhibited diurnal fluctuation (**b**) and were significantly greater in the dark period compared to the light period (□ in **c**; $n = 6$; two-tailed t-test). (**d**) ISF $A\beta_{1\text{-}x}$ levels were correlated with ISF lactate levels throughout the sleep/wake cycle (Pearson $r = 0.6351$; $P < 0.0001$). *, $P < 0.05$; **, $P < 0.01$. Values represent mean ± SEM.

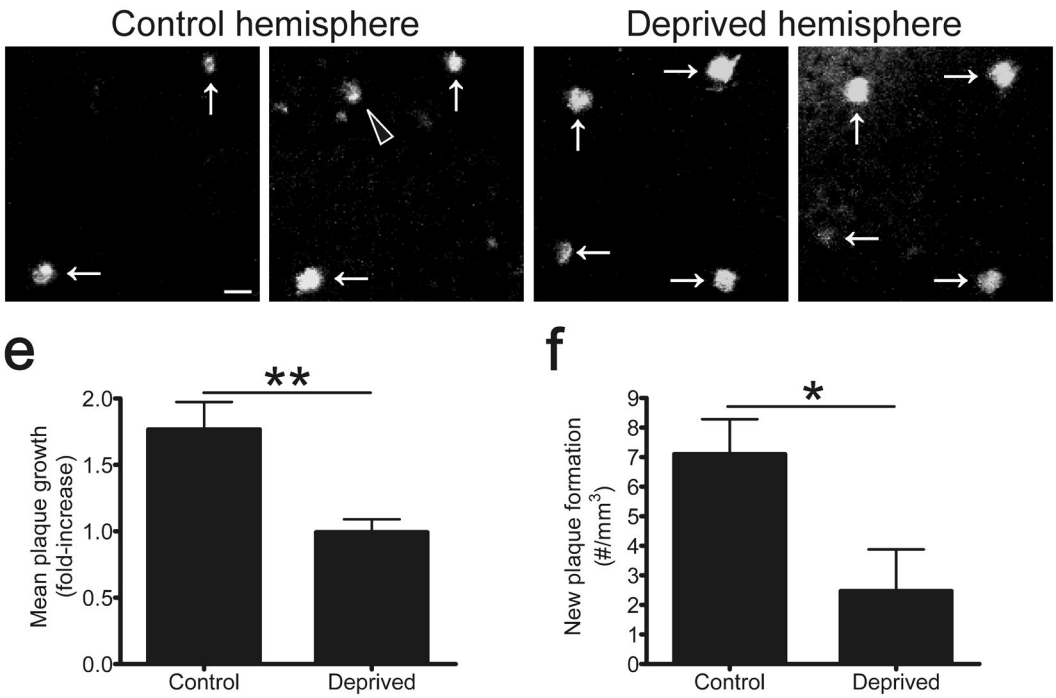

Figure 7.

Vibrissae deprivation reduces amyloid plaque growth and formation in vivo. (**a**,**b**) Representative multiphoton micrographs of individual amyloid plaques in barrel cortex in control hemisphere of APP/PS1 mice before (**a**) and after (**b**) 28 days of unilateral vibrissae deprivation. (**c**,**d**) Representative multiphoton micrographs of amyloid plaques in barrel cortex in vibrissae-deprived hemisphere of APP/PS1 mice before (**c**) and after (**d**) 28 days of vibrissae deprivation. (**e**) Long-term vibrissae deprivation decreased existing amyloid plaque growth compared to the control hemisphere (n = 6 mice; two-tailed t-test). (**f**) Long-term vibrissae deprivation also reduced new plaque formation compared to the control hemisphere (n = 6 mice; two-tailed t-test). ↑, existing amyloid plaque; △, newly formed amyloid plaque. Scale bar, 50 μM; *, $P < 0.05$; **, $P < 0.01$. Values represent mean ± SEM.